

Chemically Self-Consistent Modeling of the Globular Cluster NGC 2808 and its Effects on the Inferred Helium abundance of Multiple Stellar Populations.

EMILY M. BOUDREAUX,¹ BRIAN C. CHABOYER,¹ REHNATA HOH,¹ AND GREGORY FEIDEN²

¹*Department of Physics and Astronomy, Dartmouth College, Hanover, NH 03755, USA*

²*Department of Physics and Astronomy, University of North Georgia, Dahlonega, GA 30533, USA*

ABSTRACT

Globular Clusters (GCs) provide a unique astrophysical laboratory for studying the formation and evolution of stars. GCs are old, dense, and it has historically been believed that they have a single stellar population. However, in the last two decades, it has been definitively shown that most if not all Milky Way GCs have multiple stellar populations (MPs). These MPs are chemically distinct from one another, primarily separated by light element, including helium, abundance variations without the standard accompanying heavy element abundance variations. As the precise formation channel of these MPs remains an open question, and one which is sensitive to the population - population compositional differences, the extent of the composition variations between MPs is a key parameter to constrain. Many metal abundances may be directly measured spectroscopically; however, helium abundances are not directly observable in GCs. Instead, helium abundances are inferred from stellar models. It is therefore important to understand build stellar models that are self-consistent in the compositions of the structure, atmosphere, and opacity. In this work we present the first chemically self-consistent stellar models of the Milky Way Globular Cluster NGC 2808 using MARCS model atmospheres, OPLIB high-temperature radiative opacities, and AESOPUS low-temperature radiative opacities. We find that the helium abundance of the second generation of stars is higher than the first generation by **SOME AMOUNT**. This is in agreement with previous studies of NGC 2808.

Keywords: Globular Clusters (656), Stellar evolutionary models (2046)

1. INTRODUCTION

Globular clusters (GCs) are among the oldest observable objects in the universe (Peng et al. 2011). They are characterized by high densities with typical half-light radii of ≤ 10 pc (van den Bergh 2010), and typical masses ranging from 10^4 – 10^5 M_\odot (Brodie & Strader 2006) — though some GCs are significantly larger than these typical values **EXAMPLE**. GCs provide a unique way to probe stellar evolution (Baumgardt & Makino 2003), galaxy formation models (Boylan-Kolchin 2018; Kravtsov & Gnedin 2005), and dark matter halo structure (Hudson & Robison 2018). **BRING IN SOME MORE RECENT CITATIONS.**

The traditional view of Globular Clusters was, for a long time, that they consisted of a single stellar population (SSP, in some publications this is referred to as a Simple Stellar Population). This view was supported by spectroscopically uniform heavy element abundances (?) **[CHECK]**, and the lack of evidence for multiple stellar populations (MPs) in the color-magnitude diagrams of GCs (?). However, in the last two decades, it has been definitively shown that most if not all Milky Way GCs have MPs (Piotto et al. 2015). The lack of photometric evidence for MPs can be attributed to the short color throw available to ground based photometric surveys (?). While MPs are chemically distinct from one another, that distinction is most prominent when observing with U and B filters (Sbordone et al. 2011).

The prevalence of multiple populations in GCs is so distinct that the proposed definitions for what constitutes a globular cluster now often center the existence of MPs. Whereas, people have often tried to categorized objects as GCs through relations between half-

Corresponding author: Emily M. Boudreaux
emily.m.boudreaux.gr@dartmouth.edu,
emily@boudreauxmail.com

light radius, density, and surface brightness profile, in fact many objects which are generally thought of as GCs don't cleanly fit into these cuts **EXAMPLE + CITATION**. Consequently, Carretta et al. (2010) proposed a definition of GC based on observed chemical inhomogeneities in their stellar populations. The modern understanding of GCs then is not simply one of a dense cluster of stars which may have chemical inhomogeneities and multiple populations; rather, it is one where those chemical inhomogeneities and multiple populations themselves are the defining element of a GC.

All Milky Way globular clusters older than 2 Gyr studied in detail show populations enriched in He, N, and Na while also being depleted in O and C (Piotto et al. 2015; Bastian & Lardo 2018). These light element abundance patterns also are not strongly correlated with variations in heavy element abundance, resulting in spectroscopically uniform Fe abundances between populations. Further, high-resolution spectral studies reveal anti-correlations between N-C abundances, Na-O abundances, and potentially Al-Mg (Snedden et al. 1992; Gratton et al. 2012). Typical stellar fusion reactions can deplete core oxygen; however, the observed abundances of Na, Al, and Mg cannot be explained by the likes of the CNO cycle (Prantzos et al. 2007).

Formation channels for these multiple populations remain a point of debate among astronomers. Most proposed formation channels consist of some older, more massive, population of stars polluting the pristine cluster media before a second population forms, now enriched in heavier elements which they themselves could not have generated (for a detailed review see Gratton et al. 2012). The four primary candidates for these polluters are asymptotic giant branch stars (AGBs, Ventura et al. 2001; D'Ercole et al. 2010), fast rotating massive stars (FRMSs, Decressin et al. 2007), super massive stars (SMSs, Denissenkov & Hartwick 2014), and massive interacting binaries (MIBs, de Mink et al. 2009; Bastian & Lardo 2018).

Hot hydrogen burning (proton capture), material transport to the surface, and material ejection into the intra-cluster media are features of each of these models and consequently they can all be made to *qualitatively* agree with the observed elemental abundances. However, none of the standard models can currently account for all specific abundances (Gratton et al. 2012). AGB and FRMS models are the most promising; however, both models have difficulty reproducing severe O depletion (Ventura & D'Antona 2009; Decressin et al. 2007). Moreover, AGB and FRMS models require significant mass loss ($\sim 90\%$) between cluster formation and the current epoch — implying that a significant fraction of

halo stars formed in GCs (Renzini 2008; D'Ercole et al. 2008; Bastian & Lardo 2015).

In addition to the light-element anti-correlations observed it is also known that younger populations are significantly enhanced in Helium (Piotto et al. 2007, 2015; Latour et al. 2019). Depending on the cluster, Helium mass fractions as high as $Y = 0.4$ have been inferred (e.g. Milone et al. 2015). However, due to the relatively high and tight temperature range of partial ionization for He it cannot be observed in globular clusters; consequently, the evidence for enhanced He in GCs originates from comparison of theoretical stellar isochrones to the observed color-magnitude-diagrams of globular clusters. Therefore, a careful handling of chemistry is essential when modeling with the aim of discriminating between MPs; yet, only a very limited number of GCs have yet been studied with chemically self-consistent (structure and atmosphere) isochrones (e.g. Dotter et al. 2015, NGC 6752).

NGC 2808 is the prototype globular cluster to host Multiple Populations. Various studies since 2007 have identified that it may host anywhere from 2-5 stellar populations. These populations have been identified both spectroscopically (i.e.) and photometrically (i.e.). Note that recent work (Valle et al. 2022) calls into question the statistical significance of the detections of more than 2 populations in the spectroscopic data. Here we present new, chemically self-consistent modeling of the photometry of the two extreme populations of NGC 2808 identified by Milone et al. (2015), populations A and E. **Additionally, we present a likelihood analysis of the photometric data of NGC 2808 to determine the number of populations present in the cluster.**

2. CHEMICAL CONSISTENCY

There are three primary areas in which must the stellar models must be made chemically consistent: the atmospheric boundary conditions, the opacities, and interior abundances. The interior abundances are relatively easily handled by adjusting parameters within our stellar evolutionary code. However, the other two areas are more complicated to bring into consistency. Atmospheric boundary conditions and opacities must both be calculated with a consistent set of chemical abundances outside of the stellar evolution code. For evolution we use the Dartmouth Stellar Evolution Program (DSEP) (Dotter et al. 2008), a well tested 1D stellar evolution code which has a particular focus on modelling low mass stars ($\leq 2 M_{\odot}$)

2.1. Atmospheric Boundary Conditions

Certain assumptions, primarily that the radiation field is at equilibrium and radiative transport is diffusive

(Salaris & Cassisi 2005), made in stellar structure codes, such as DSEP, are valid when the optical depth of a star is small. However, in the atmospheres of stars, the number density of particles drops low enough and the optical depth consequently becomes large enough that these assumptions break down, and separate, more physically motivated, plasma modeling code is required. Generally structure code will use tabulated atmospheric boundary conditions generated by these specialized codes ATLAS9 (Kurucz 1993), PHEONIX (Husser et al. 2013), MARCS (Gustafsson et al. 2008), and MPS-ATLAS (Kotogryz et al. 2023). Often, as the boundary conditions are both expensive to compute and not the speciality of stellar structure researchers, the boundary conditions are not updated as as light-element interior abundance varies.

One key element when chemically consistently modeling NGC 2808 modeling is the incorporation of new atmospheric models with the same elemental abundances as the structure code. We use atmospheres generated from the MARCS grid of model atmospheres (Plez 2008). MARCS provides one-dimensional, hydrostatic, plane-parallel and spherical LTE atmospheric models (Gustafsson et al. 2008). Model atmospheres are made to match the spectroscopically measured elemental abundances of populations A and E. Moreover, for each populations, atmospheres with various helium mass fractions are generated. These range from $Y=0.24$ to $Y=0.36$ in steps of 0.02. A comparison of the pressure and temperature throughout the atmospheres of the two populations with helium abundances representative of literature values is shown in Figure 2.1.

2.2. Opacities

In addition to the atmospheric boundary conditions, both the high and low temperature opacities used by DSEP must be made chemically consistent. Here we use OPLIB high temperature opacity tables (Colgan et al. 2016) retrieved using the TOPS web-interface. Low temperature opacity tables are retrieved from the Aesopus 2.0 web-interface (Marigo & Aringer 2009; Marigo et al. 2022). Ideally, these opacities would be the same used in the atmospheric models. However, the opacities used in the MARCS models are not publicly available. As such, we use the opacities provided by the TOPS and Aesopus 2.0 web-interfaces.

3. STELLAR MODELS

We use the Dartmouth Stellar Evolution Program (DSEP, Dotter et al. 2008) to generate stellar models. DSEP is a well-tested, one-dimensional stellar evolution code which includes a mixing length model of convection, gravitational settling, and diffusion.

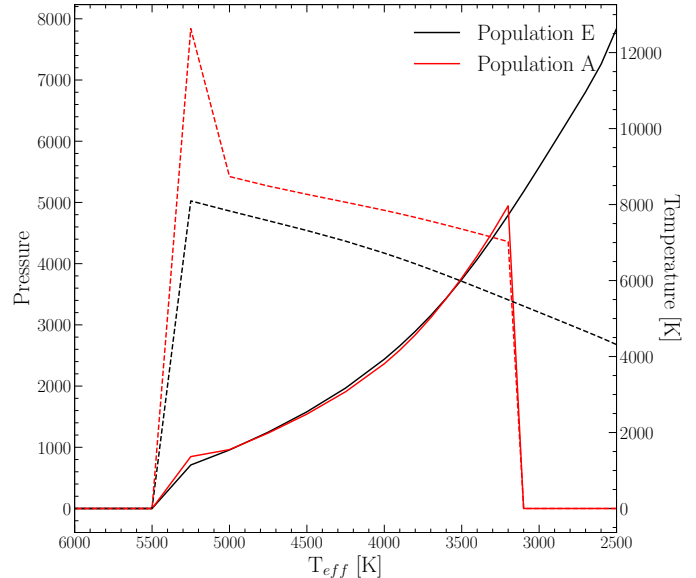


Figure 1. Comparison of the MARCS model atmospheres generated for the two extreme populations of NGC 2808. These lines shows population A and E with the same Helium abundance; though, we fit a grid of models over various helium abundances. Dashed lines show the temperature of the boundary condition while solid lines show the pressure.

We use DSEP to evolve stellar models ranging in mass from 0.3 to 2.0 solar masses from the zero-age main sequence (ZAMS) to the tip of the red giant branch. Below $0.7 M_{\odot}$ we evolve a model every $0.03 M_{\odot}$ and above $0.7 M_{\odot}$ we evolve a model every $0.5 M_{\odot}$. Additionally, we evolve models over a grid of mixing length parameters, α_{MLT} , from $\alpha_{MLT} = 1.0$ to $\alpha_{MLT} = 2.0$ in steps of 0.1. In addition to the mixing length grid the evolved grid of models also has dimensions population (A or E) and helium abundance (Y). Each model is evolved in DSEP’s “high resolution” mode and had a maximum allowed time step of 50 Myr.

Table here of the abundances of population A and E, cite (Milone et al. 2015). These should be presented as $a(H)=12$, and so on correct?

For each combination of population, Y , and α_{MLT} we use the isochrone generation code first presented in ? to generate a grid of isochrones. The isochrone generation code identified equivalent evolutionary points (EEPs) over a series of masses and interpolates between them. The grid of isochrones generated for this work is available as a digital supplement to this paper.

4. FIDANKA

When fitting isochrones to the data we have four main criteria for any method

- The method must be robust enough to work along the entire main sequence, turn off, and much of the subgiant and red giant branches.
- Any method should consider photometric uncertainty in the fitting process.
- The method should be model independent, weighting any n number of populations equally.
- The method should be automated and require minimal intervention from the user.

We do not believe that any currently available software is a match for our use case. Therefore, we elect to develop our own software suite, **Fidanka**. **Fidanka** is a python package designed to automate much of the process of measuring fiducial lines in CMDs, adhering to the four criteria we lay out above. Primary features of **Fidanka** may be separated into three primary categories: fiducial line measurement, stellar population synthesise, and isochrone optimization/fitting. Additionally, there are utility functions which are detailed in the **Fidanka** documentation.

4.1. Fiducial Line Measurement

Fidanka takes an iterative approach to measuring fiducial lines, the first step of which is to make a “guess” as to the fiducial line. This initial guess is calculated by splitting the CMD into magnitude bins, with uniform numbers of stars per bin (so that bins cover a small magnitude range over densely populated regions of the CMD while covering a much larger magnitude range in sparsely populated regions of the CMD, such as the RGB). A unimodal Gaussian distribution is then fit to the color distribution of each bin, and the resulting mean color is used as the initial fiducial line guess. This rough fiducial line will approximately trace the area of highest density. The initial guess will be used to verticalize the CMD so that further algorithms can work in 1-D magnitude bins without worrying about weighting issues caused by varying projections of the evolutionary sequence onto the magnitude axis. Verticalization is performed taking the difference between the guess fiducial line and the color of each star in the CMD.

If **Fidanka** were to simply apply the same algorithm to the verticalized CMD then the resulting fiducial line would likely be a re-extraction of the initial fiducial line guess. To avoid this, we take a more robust, number density based approach, which considers the distribution of stars in both color and magnitude space simultaneously. For each star in the CMD we first use an **introselect** partitioning algorithm to select the 50th nearest stars. To account for the case where the star is

at an extreme edge of the CMD, those 50 stars include the star itself (such that we really select 49 stars + 1). We use **qhull**¹ (Barber et al. 1996; ?) to calculate the convex hull of those 50 points. The number density at each star then is defined as $50/A_{hull}$, where A_{hull} is the area of the convex hull. Because we use a fixed number of points per star, and a partitioning algorithm as opposed to a sorting algorithm, this method scales like $O(n)$, where n is the number of stars in the CMD. This method also intrinsically weights the density of each star equally as the counting statistics per bin are uniform. We are left with a CMD where each star has a defined number density (Figure 4.1).

Fidanka can now exploit this density map to fit a better fiducial line to the data, as the density map is far more robust to outliers. There are multiple algorithms we implement to fit the fiducial line to the color-density profile in each magnitude bin (Figure 4.1); they are explained in more detail in the **Fidanka** documentation. However, of most relevance here is the Bayesian Gaussian Mixture Modeling (BGMM) method. BGMM is a clustering algorithm which, for some fixed number of n-dimensional Gaussian distributions, K , determines the mean, covariance, and mixing probability (somewhat analogous to amplitude) of each k^{th} distribution, such that the local lower bound of the evidence of each star belonging strongly to a single distribution is maximized.

Maximization is performed using the Dirichlet process, which is a non-parametric Bayesian method of determining the number of Gaussian distributions, K , which best fit the data [CITATION]. Use of the Dirichlet process allows for dynamic variation in the number of inferred populations from magnitude bin to magnitude bin. Specifically, populations are clearly visually separated from the lower main sequence through the turn off; however, at the turn off and throughout much of the subgiant branch, the two visible populations overlap due to their extremely similar ages (Citation). The Dirichlet process allows for the BGMM method to infer a single population in these regions, while inferring two populations in regions where they are clearly separated. More generally, the use of the Dirichlet process removes the need for a prior on the exact number of populations to fit. Rather, the user specifies an upper bound on the number of populations within the cluster. An example bin (F814W = 20.6) is shown in Figure 4.

Fidanka’s BGMM method first breaks down the verticalized CMD into magnitude bins with uniform numbers of stars per bin (here we adopt 250). Any stars

¹ <https://www.qhull.com>

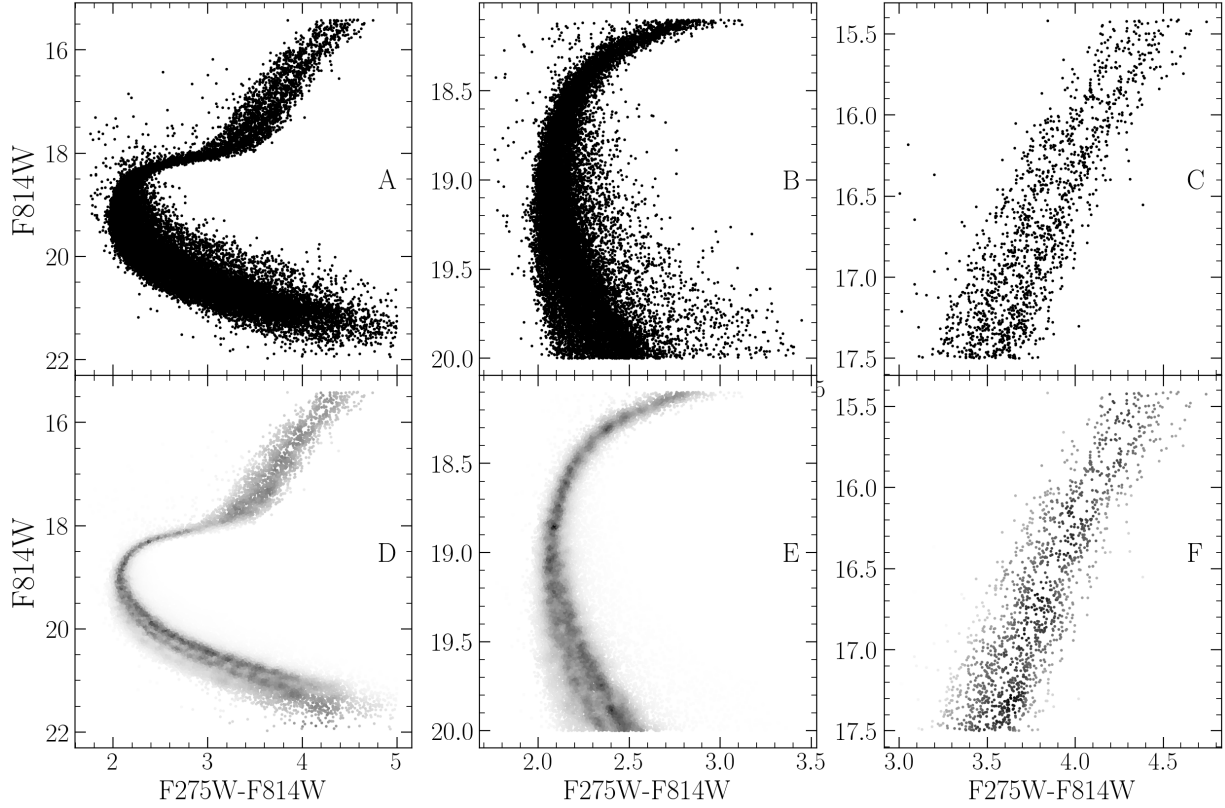


Figure 2. Density map demo showing density estimate over different parts of the evolutionary sequence. The left panel shows the density map over the entire evolutionary sequence, while the middle panel shows the density map over the main sequence and the right most panel shows the density map over the RGB. Figures in the top row are the raw CMD, while figures in the bottom row are colored by the density map.

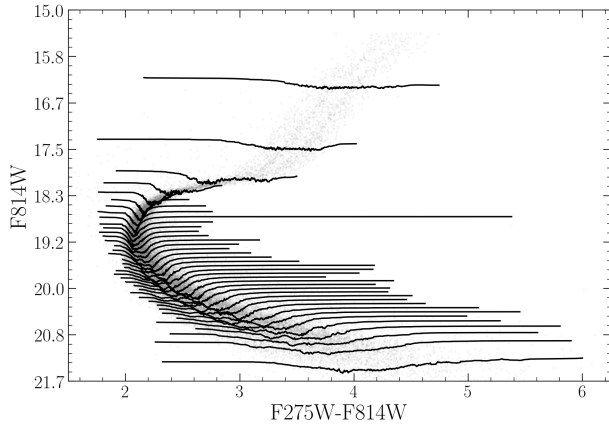


Figure 3. CMD where points are colored by density. Lines show the density-color profile in each magnitude bin. In this figure adaptive binning targeted 1000 stars per bin

left over are placed into the final bin. For each bin a BGMM model with a maximum of 5 populations is fit to the color density profile. The number of populations is then inferred from the weighting parameter (the mixing probability) of each population. If the weighting parameter of any k^{th} components less than 0.05, then that

component is considered to be spurious and removed. Additionally, if the number of populations in the bin above and the bin below are the same, then the number of populations in the current bin is forced to be the same as the number of populations in the bin above. Finally, the initial guess fiducial line is added back to the BGMM inferred line. Figure 5 shows the resulting fiducial line(s) in each magnitude bin for both a verticalized CMD and a non verticalized CMD.

This method of fiducial line extraction effectively discriminated between multiple populations along the main sequence and RGB of a cluster, while simultaneously allowing for the presence of a single population along the MSTO and subgiant branch.

We can adapt this density map based BGMM method to consider photometric uncertainties by adopting a simple Monte Carlo approach. Instead of measuring the fiducial line(s) a single time, *Fidanka* can measure the fiducial line(s) many times, resampling the data with replacement each time. For each resampling *Fidanka* adds a random offset to each filter based on the photometric uncertainties of each star. From these n measurements the mean fiducial line for each sequence can be identified

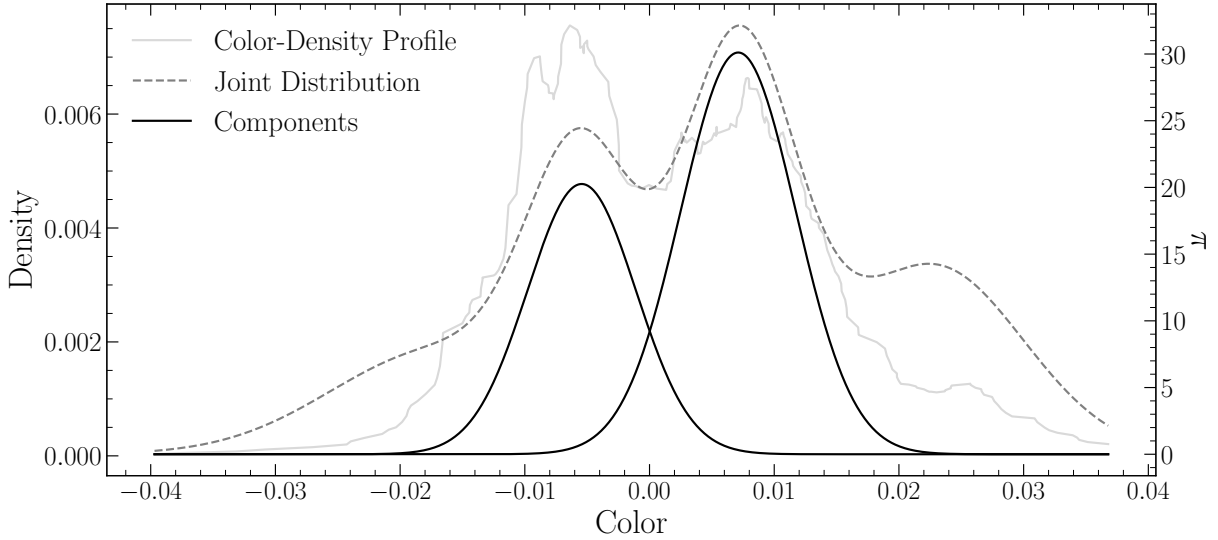


Figure 4. Example of BGMM fit to a magnitude bin. The grey line shows the underlying color-density profile, while the black dashed-line shows the joint distribution of each BGMM component. The solid black lines show the two selected components.

along with upper and lower bound confidence intervals in each magnitude bin.

4.2. Stellar Population Synthesis

In addition to measuring fiducial lines, **Fidanka** also includes a stellar population synthesise module. This module is used to generate synthetic CMDs from a given set of isochrones. This is of primary importance for binary population modelling. The module is also used to generate synthetic CMDs for the purpose of testing the fiducial line extraction algorithms against priors.

Fidanka uses MIST formatted isochrones [CITATION] as input along with distance modulus, B-V color excess, binary mass fraction, and bolometric corrections. An arbitrarily large number of isochrones may be used to define an arbitrary number of populations. Synthetic stars are samples from each isochrone based on a definable probability (for example it is believed that $\sim 90\%$ of stars in globular clusters are younger population [CITATION]). Based on the metallicity, μ , and $E(B-V)$ of each isochrone, bolometric corrections are taken from bolometric correction tables. Where bolometric correction tables do not include exact metallicities or extinctions a linear interpolation is performed between the two bounding values. [FIGURE] shows an example of a synthetic CMD generated from a set of 2 NGC 2808 isochrones as well as a comparison between those isochrones and the measured fiducial line of the synthetic population.

4.3. Isochrone Optimization

The optimization routines in **Fidanka** will find the best fit distance modulus, B-V color excess, and binary

number fraction for a given set of isochrones. If a single isochrone is provided then the optimization is done by minimizing the χ^2 of the perpendicular distances between an isochrone and a fiducial line. If multiple isochrones are provided then those isochrones are first used to run stellar population synthesis and generate a synthetic CMD. The optimization is then done by minimizing the χ^2 of both the perpendicular distances between and widths of the observed fiducial line and the fiducial line of the synthetic CMD.

4.4. Fidanka Testing

In order to validate **Fidanka** we have run an series of injection recovery tests using **Fidanka**'s population synthesis routines to build various synthetic populations and **Fidanka**'s fiducial measurement routines to recover these populations. We run multiple tests in order to validate **Fidanka**'s ability to extract varying numbers of populations without the prior of the exact population number. Table ?? provides the parameters for each injection recovery test along with the χ^2 difference between each isochrone and its associated fiducial line.

Each population was generated using either a salpeter initial mass function (Salpeter 1955) or the initial mass function given in (Milone et al. 2012) ($\alpha = -1.2$ redmost population and $\alpha = -0.9$ for the bluemost and second bluemost populations). Every population was assumed to have a binary population fraction of 10%, to have a distance of 0pc and to have a B-V color excess of 0. Finally, each synthetic population was generated using a fixed age of 12 Gyr.

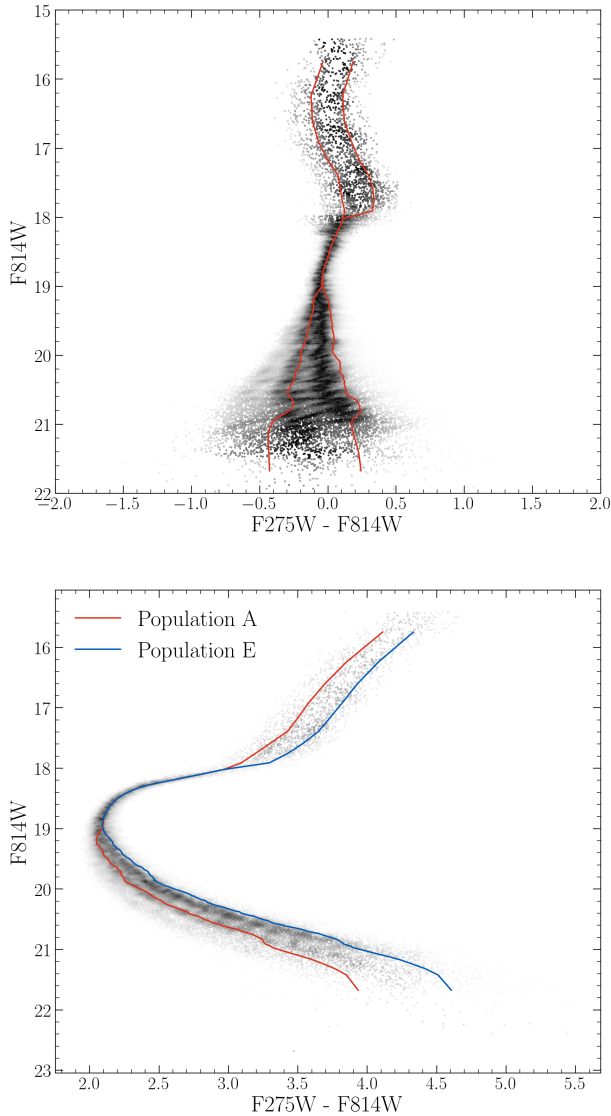


Figure 5. CMD where points are colored by density. Line trace the inferred fiducial line(s) in each magnitude bin.

The top panel Figure ?? shows the populations generated for these tests. while the bottom panel shows the populations with the density variations highlighted.

We measure the fiducial lines in these populations using *Fidanka*’s fiducial measurement utility. For the same reasons as outlined in Section ?? we use the F275W and F814W filters. A maximum population number is set at 5 for each trial. Figure ?? shows the fiducial lines on top of each synthetic population. Recall from Section ?? that use of Bayesian Gaussian Mixture Modeling (BGMM) allows us to predict the optimal number of populations to recreate a distribution; therefore, where you see a single line BGMM has predicted only one population is needed whereas when you see 2 lines BGMM has predicted that 2 populations are needed. Importantly,

these population numbers are not hard coded into our injection and recovery tests.

The efficacy of the fiducial measurement is evaluated by calculating the χ^2 metric between the fiducial line and isochrone over 0.1 mag bins. This allows us to probe which portions of the evolutionary sequence contribute most to the overall χ^2 difference (Figure ??).

5. ISOCHRONE FITTING

We fit pairs of isochrones to the HUGS data for NGC 2808 using *Fidanka*, as described in §FIDANKA SECTION. Two isochrones, one for Population A and one for Population E are fit simultaneously. These isochrones are constrained to have the same distance modulus, μ , and color excess, $E(B-V)$. Moreover, we constrain the mixing length, α_{ML} , to be constant between any two isochrones in a set. For every isochrone in the set of combination of which fulfilling these constraints μ , $E(B-V)$, Age_A , and Age_E are optimized to reduce the χ^2 distance between the fiducial lines and the isochrones. Because we fit fiducial lines directly, we do not need to consider the binary population fraction, f_{bin} , as a free parameter.

Table ?? shows the results of the isochrone fitting for NGC 2808. The best fit isochrones are shown in Figure ??.

Discuss the implications of the specific isochrones we fit.

5.1. ACS-HUGS Photometric Zero Point Offset

The Hubble legacy archive photometry used in this work is calibrated to the Vega magnitude system. However, we have found that the photometry has a systematic offset of ~ 0.02 magnitudes in the F814W band when compared to the same stars in the ACS survey [CITATION]. The exact cause of this offset is unknown, but it is likely due to a difference in the photometric zero point between the two surveys. A full correction of this offset would require a careful re-reduction of the HUGS photometry, which is beyond the scope of this work. We instead recognize a 0.02 inherent uncertainty in the inferred magnitude of any fit when comparing to the ACS survey. This uncertainty is small when compared to the uncertainty in the distance modulus and should not affect the conclusion of this paper.

Figure Showing the offset

The independent analysis of the Hubble Space Telescope photometry ACS and HUGS, and an additional ground-based dataset created by Stetson et al. (2009), of the globular cluster NGC2808 resulted in findings of a systematic difference in the magnitude of the stars. A significant offset between the three datasets was found. HUGS and ACS were found to have consistent data for

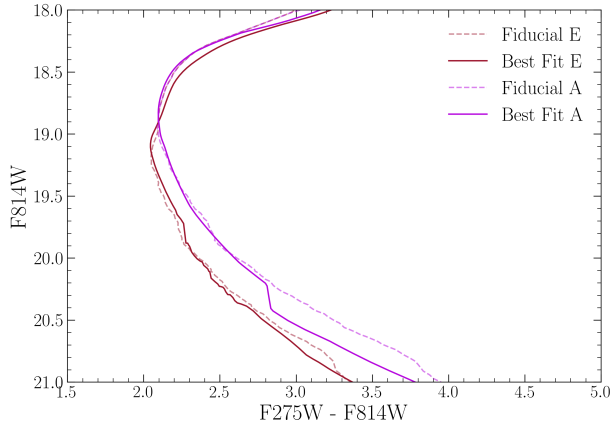


Figure 6. Best fit isochrone results for NGC 2808.

Vvega, however an offset of approximately 0.025 was found in the Ivega. ACS and Stetson were found to have inconsistent differences in both Vvega and Ivega. The three photometric studies do not match, and future studies which compare theoretical models to the data will need to take into account these systematic uncertainties.

6. RESULTS

Using **Fidanka** we fit pairs of Population A + E isochrones to the HUGS data for NGC 2808. Each pair of isochrones is allowed to vary in distance modulus, red-

dening, relative helium mass fraction (A/E), and age. Any population pairs which vary by more than 1% in distance modulus or B-V color excess are rejected. The χ^2 distribution for the isochrone pairs is shown in Figure [FIGURE]. The best fit isochrones are shown in Figure 6 and optimized parameters for these are presented in Table [TABLE].

Need to make the chi2 dist plot still. Have all these values but need to figure out best way to visualize it

Currently are still seeing a discontinuity in the isochrone below the MSTO. This must be addressed before submission.

7. CONCLUSION

Here we have performed the first chemically self-consistent modeling of the Milky Way Globular Cluster NGC 2808. We find that, updated atmospheric boundary conditions and opacity tables do not have a significant effect on the inferred helium abundances of multiple populations.

This work has made use of the NASA astrophysical data system (ADS). We would like to thank Elisabeth Newton and Aaron Dotter for their support and for useful discussion related to the topic of this paper. Additionally, we would like to thank Kara Fagerstrom, Aylin Garcia Soto, and Keighley Rockcliffe for their useful discussion related to in this work. We acknowledge the support of a NASA grant (No. 80NSSC18K0634).

REFERENCES

- Barber, C. B., Dobkin, D. P., & Huhdanpaa, H. 1996, ACM Transactions on Mathematical Software (TOMS), 22, 469
- Bastian, N., & Lardo, C. 2015, MNRAS, 453, 357, doi: [10.1093/mnras/stv1661](https://doi.org/10.1093/mnras/stv1661)
- Bastian, N., & Lardo, C. 2018, Annual Review of Astronomy and Astrophysics, 56, 83
- Baumgardt, H., & Makino, J. 2003, MNRAS, 340, 227, doi: [10.1046/j.1365-8711.2003.06286.x](https://doi.org/10.1046/j.1365-8711.2003.06286.x)
- Boylan-Kolchin, M. 2018, MNRAS, 473, 1423, doi: [10.1093/mnras/sty1490](https://doi.org/10.1093/mnras/sty1490)
- Brodie, J. P., & Strader, J. 2006, Annu. Rev. Astron. Astrophys., 44, 193
- Carretta, E., Bragaglia, A., Gratton, R. G., et al. 2010, Astronomy & Astrophysics, 516, A55
- Colgan, J., Kilcrease, D. P., Magee, N. H., et al. 2016, in APS Meeting Abstracts, Vol. 2016, APS Division of Atomic, Molecular and Optical Physics Meeting Abstracts, D1.008
- de Mink, S. E., Pols, O. R., Langer, N., & Izzard, R. G. 2009, A&A, 507, L1, doi: [10.1051/0004-6361/200913205](https://doi.org/10.1051/0004-6361/200913205)
- Decressin, T., Meynet, G., Charbonnel, C., Prantzos, N., & Ekström, S. 2007, A&A, 464, 1029, doi: [10.1051/0004-6361:20066013](https://doi.org/10.1051/0004-6361:20066013)
- Denissenkov, P. A., & Hartwick, F. D. A. 2014, MNRAS, 437, L21, doi: [10.1093/mnras/slt133](https://doi.org/10.1093/mnras/slt133)
- D’Ercole, A., D’Antona, F., Ventura, P., Vesperini, E., & McMillan, S. L. W. 2010, MNRAS, 407, 854, doi: [10.1111/j.1365-2966.2010.16996.x](https://doi.org/10.1111/j.1365-2966.2010.16996.x)
- D’Ercole, A., Vesperini, E., D’Antona, F., McMillan, S. L. W., & Recchi, S. 2008, MNRAS, 391, 825, doi: [10.1111/j.1365-2966.2008.13915.x](https://doi.org/10.1111/j.1365-2966.2008.13915.x)
- Dotter, A., Chaboyer, B., Jevremović, D., et al. 2008, The Astrophysical Journal Supplement Series, 178, 89
- Dotter, A., Ferguson, J. W., Conroy, C., et al. 2015, MNRAS, 446, 1641, doi: [10.1093/mnras/stu2170](https://doi.org/10.1093/mnras/stu2170)

- 560 Gratton, R. G., Carretta, E., & Bragaglia, A. 2012,
 561 *Astronomy and Astrophysics Reviews*, 20, 50,
 562 doi: [10.1007/s00159-012-0050-3](https://doi.org/10.1007/s00159-012-0050-3)
- 563 Gustafsson, B., Edvardsson, B., Eriksson, K., et al. 2008,
 564 *A&A*, 486, 951, doi: [10.1051/0004-6361:200809724](https://doi.org/10.1051/0004-6361:200809724)
- 565 Hudson, M. J., & Robison, B. 2018, *Monthly Notices of the*
 566 *Royal Astronomical Society*, 477, 3869,
 567 doi: [10.1093/mnras/sty844](https://doi.org/10.1093/mnras/sty844)
- 568 Husser, T. O., Wende-von Berg, S., Dreizler, S., et al. 2013,
 569 *A&A*, 553, A6, doi: [10.1051/0004-6361/201219058](https://doi.org/10.1051/0004-6361/201219058)
- 570 Kostogryz, N., Shapiro, A. I., Witzke, V., et al. 2023,
 571 *Research Notes of the AAS*, 7, 39,
 572 doi: [10.3847/2515-5172/acc180](https://doi.org/10.3847/2515-5172/acc180)
- 573 Kravtsov, A. V., & Gnedin, O. Y. 2005, *The Astrophysical*
 574 *Journal*, 623, 650
- 575 Kurucz, R.-L. 1993, *Kurucz CD-Rom*, 13
- 576 Latour, M., Husser, T. O., Giesers, B., et al. 2019, *A&A*,
 577 631, A14, doi: [10.1051/0004-6361/201936242](https://doi.org/10.1051/0004-6361/201936242)
- 578 Marigo, P., & Aringer, B. 2009, *A&A*, 508, 1539,
 579 doi: [10.1051/0004-6361/200912598](https://doi.org/10.1051/0004-6361/200912598)
- 580 Marigo, P., Aringer, B., Girardi, L., & Bressan, A. 2022,
 581 *ApJ*, 940, 129, doi: [10.3847/1538-4357/ac9b40](https://doi.org/10.3847/1538-4357/ac9b40)
- 582 Milone, A. P., Piotto, G., Bedin, L. R., et al. 2012, *ApJ*,
 583 744, 58, doi: [10.1088/0004-637X/744/1/58](https://doi.org/10.1088/0004-637X/744/1/58)
- 584 Milone, A. P., Marino, A. F., Piotto, G., et al. 2015, *ApJ*,
 585 808, 51, doi: [10.1088/0004-637X/808/1/51](https://doi.org/10.1088/0004-637X/808/1/51)
- 586 Peng, E. W., Ferguson, H. C., Goudfrooij, P., et al. 2011,
 587 *The Astrophysical Journal*, 730, 23
- 588 Piotto, G., Bedin, L. R., Anderson, J., et al. 2007, *The*
 589 *Astrophysical Journal Letters*, 661, L53,
 590 doi: [10.1086/518503](https://doi.org/10.1086/518503)
- 591 Piotto, G., Milone, A. P., Bedin, L. R., et al. 2015, *AJ*, 149,
 592 91, doi: [10.1088/0004-6256/149/3/91](https://doi.org/10.1088/0004-6256/149/3/91)
- 593 Plez, B. 2008, *Physica Scripta Volume T*, 133, 014003,
 594 doi: [10.1088/0031-8949/2008/T133/014003](https://doi.org/10.1088/0031-8949/2008/T133/014003)
- 595 Prantzos, N., Charbonnel, C., & Iliadis, C. 2007, *A&A*, 470,
 596 179, doi: [10.1051/0004-6361:20077205](https://doi.org/10.1051/0004-6361:20077205)
- 597 Renzini, A. 2008, *Monthly Notices of the Royal*
 598 *Astronomical Society*, 391, 354,
 599 doi: [10.1111/j.1365-2966.2008.13892.x](https://doi.org/10.1111/j.1365-2966.2008.13892.x)
- 600 Salaris, M., & Cassisi, S. 2005, *Evolution of stars and*
 601 *stellar populations* (John Wiley & Sons)
- 602 Salpeter, E. E. 1955, *ApJ*, 121, 161, doi: [10.1086/145971](https://doi.org/10.1086/145971)
- 603 Sbordone, L., Salaris, M., Weiss, A., & Cassisi, S. 2011,
 604 *Astronomy & Astrophysics*, 534, A9
- 605 Sneden, C., Kraft, R. P., Prosser, C. F., & Langer, G. 1992,
 606 *The Astronomical Journal*, 104, 2121
- 607 Valle, G., Dell’Omodarme, M., & Tognelli, E. 2022, *A&A*,
 608 658, A141, doi: [10.1051/0004-6361/202142454](https://doi.org/10.1051/0004-6361/202142454)
- 609 van den Bergh, S. 2010, *The Astronomical Journal*, 140,
 610 1043, doi: [10.1088/0004-6256/140/4/1043](https://doi.org/10.1088/0004-6256/140/4/1043)
- 611 Ventura, P., & D’Antona, F. 2009, *A&A*, 499, 835,
 612 doi: [10.1051/0004-6361/200811139](https://doi.org/10.1051/0004-6361/200811139)
- 613 Ventura, P., D’Antona, F., Mazzitelli, I., & Gratton, R.
 614 2001, *ApJL*, 550, L65, doi: [10.1086/319496](https://doi.org/10.1086/319496)